Phytomedicine 139 (2025) 156504

Contents lists available at ScienceDirect

Phytomedicine

journal homepage: www.elsevier.com/locate/phymed

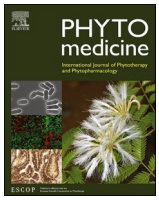

Original Article

Sclareol improves the pathology of Alzheimer's disease by inhibiting microglial inflammation via interacting with CDK9

Hao Tang [a,b,1], Luyao Li [c,1], Qin Yu [a], Linjie Chen [a], Xiaoxia Xu [a], Ziyao Meng [a], Yuqing Zeng [a], Fan Chen [a], Hammad Muzaffar [a], Wei Wang [a,**], Xia Zhao [a,b,*], Guang Liang [a,b,*]

[a] Affiliated Yongkang First People's Hospital and School of Pharmaceutical Sciences, Hangzhou Medical College, Hangzhou, Zhejiang 311399, China
[b] Department of Pharmacy and Institute of Inflammation, Zhejiang Provincial People's Hospital, Affiliated People's Hospital, Hangzhou Medical College, Hangzhou, Zhejiang 310014, China
[c] School of Pharmaceutical Sciences, Wenzhou Medical University, Wenzhou, Zhejiang 325035, China

ARTICLE INFO

Keywords:
Alzheimer's disease
Sclareol
Microglial
CDK9
NF-κB
Neuroinflammation

ABSTRACT

Background: Excessive activation of microglia triggers pro-inflammatory responses, exacerbating neuronal damage and accelerating the progression of Alzheimer's disease (AD). Thus, targeting abnormal microglial activation represents a promising therapeutic strategy for AD. In this study, we identified sclareol (SCL) through compound library screening as a potent anti-inflammatory agent capable of crossing the blood-brain barrier. However, there are currently no reports on whether SCL modulates microglial inflammation or ameliorates AD pathology.

Objective: To evaluate the anti-inflammatory effects and underlying molecular mechanism of SCL on microglial-mediated inflammation and neuronal damage in AD.

Methods: Drug Affinity Responsive Target Stability (DARTS), Liquid Chromatography-Tandem Mass Spectrometry (LC-MS), protein interaction assays, Biolayer Interferometry (BLI), and molecular docking were used to explore the interaction between SCL and cyclin-dependent kinase 9 (CDK9). Behavioral tests and immunofluorescent (IF) staining were performed to assess the effects of SCL on microglial activation and AD pathology. The molecular mechanism of the anti-inflammatory effect of SCL was analyzed by interfering with CDK9.

Results: SCL significantly inhibited the release of proinflammatory mediators, reduced neuronal damage, and alleviated cognitive deficits in AD model mice. Notably, SCL demonstrated the ability to cross the blood-brain barrier (BBB), highlighting its therapeutic potential. Mechanistically, SCL binds directly to CDK9, which contributes to the inflammatory response through its interaction with NF-κB. Knockdown of CDK9 reduced the NF-κB-mediated inflammatory response, but did not have an additive effect on SCL, indicating that SCL's efficacy is mediated by CDK9 inhibition and subsequent suppression of the NF-κB signaling pathway.

Conclusion: This study demonstrates that SCL exerts neuroprotective effects in AD mice by targeting CDK9 and downstream NF-κB signaling pathway to reduce the inflammatory activation of microglia. These findings suggest that SCL is a promising candidate for the treatment of AD, offering a novel therapeutic approach to mitigate disease progression through modulation of microglial activation.

Abbreviations: AD, Alzheimer's disease; BLI, Biolayer Interferometry; BBB, blood-brain barrier; BSA, bovine serum albumin; CDK9, cyclin-dependent kinase 9; CETSA, cellular thermal shift assays; CDC37, cell division cycle 37 homolog; GWAS, Genome-wide association studies; IF, Immunofluorescent staining; IL-1β, interleukin-1β; IL-6, interleukin-6; LC-MS, Liquid Chromatography-Tandem Mass Spectrometry; MWM, Morris Water Maze; NOR, New Object Recognition; NF-κB, Nuclear Factor κB; PD, Parkinson's disease; PFA, paraformaldehyde; PI, propidium iodide; P65, P-NF-κB65; qPCR, quantitative PCR; rhCDK9, Recombinant human CDK9; SCL, sclareol; si-CDK9, CDK9-targeting siRNA; TNF-α, tumor necrosis factor-α.

* Corresponding authors at: Hangzhou Medical College, Hangzhou, Zhejiang 311399, China.
** Corresponding author at: Affiliated Yongkang First People's Hospital, Hangzhou Medical College, Yongkang, Zhejiang 321399, China.
E-mail addresses: ykoneway2000@126.com (W. Wang), xiazhao@hmc.edu.cn (X. Zhao), liangguang@wmu.edu.cn (G. Liang).
[1] These author made equal contribution to this work.

https://doi.org/10.1016/j.phymed.2025.156504
Received 27 October 2024; Received in revised form 29 December 2024; Accepted 11 February 2025
Available online 13 February 2025

Introduction

Alzheimer's disease (AD) is the most common form of dementia, associated with clinical manifestations of cognitive impairment and behavioral abnormalities (DeTure and Dickson, 2019; McKhann et al., 2011). It is expected that the global prevalence of AD will triple by 2050, placing a heavy burden on families and society (Scheltens et al., 2021). Although several synthetic drugs, such as memantine and donepezil, have been used to treat AD (Casey et al., 2010), these drugs only relieve some symptoms, do not block the progression of the disease, and have notable side effects (Knopman et al., 2021). Therefore, there is an urgent need to find effective drugs for treating AD.

The unclear pathogenesis is a key challenge in the development of drugs for AD. With in-depth research into the pathogenic mechanisms of AD, microglia and their related genes have considered to be key factors in the occurrence and development of AD. Increasing evidence shows that microglia play a crucial role in the progression of AD (Glass et al., 2010; Wang et al., 2022a). Activated microglia are the commanders of the brain tissue inflammatory state, and they excessively phagocytose the dendritic spines of neurons, leading to massive neuronal death (Lopez-Rodriguez et al., 2021). The massive death of neurons is the main cause of cognitive decline in patients (Ransohoff and Perry, 2009)' (Colonna and Butovsky, 2017). In AD cases, microglia exhibit abnormal morphology (Althafar, 2022), and those surrounding Aβ plaques stain positively for activation markers and pro-inflammatory mediators (Akiyama et al., 2000). Furthermore, microglial activation precedes the onset of Tau and Aβ pathology (Tarkowski et al., 2003; Wright et al., 2013). Genome-wide association studies (GWAS) have reported that most AD risk loci are located in genes that are occasionally unique and highly expressed in microglia (Schwartzentruber et al., 2021). These findings suggest that microglia based strategies may be a new perspective for the development of anti-AD drug candidates.

Natural products are a valuable resource for developing new compounds to treat major diseases, offering the advantage of fewer side effects and making them strong candidates for drug development (Atanasov et al., 2021; Wang et al., 2021) . Increasing research suggests that certain natural products may positively impact AD (Yang et al., 2023). Compounds such as luteolin (He et al., 2023), urolithin a (Hou et al., 2024), and artemisinin B (Qiang et al., 2018) have shown potential, although these studies have primarily focused on neuroprotection and mitochondrial dysfunction, with limited exploration of their effects on microglia. Sclareol (SCL), a natural compound derived from the Mediterranean medicinal plant *Salvia sclarea*, exhibits low systemic toxicity, good bioavailability *in vivo*, and the ability to cross the blood-brain barrier (BBB) following oral administration (Dimas et al., 1999). SCL has demonstrated various biological activities, including significant neuroprotective effects in neurodegenerative diseases such as Parkinson's disease (PD) (Wang et al., 2022b) and depression (Bappi et al., 2024). However, its role and mechanism of action in AD remain unclear.

In the present study, we investigated the role of SCL in AD using BV2 cells and 3 × Tg AD mice models. The direct molecular targets and downstream mechanisms of SCL action were further explored through mass spectrometry and immunoprecipitation techniques. Our results demonstrate that SCL mediates its effects by directly interacting with cyclin-dependent kinase 9 (CDK9), thereby inhibiting the downstream NF-κB signaling pathway. This modulation results in an enhancement of the brain's inflammatory environment and a decrease in AD pathology. In conclusion, our research indicates that SCL presents potential as a therapeutic agent for the management of AD.

Material and methods

General reagents

Sclraeol (515–03–7) was purchased from MCE (USA). Recombinant human CDK9 (rhCDK9) was purchased from Cusabio (CSB-YP005079HU, Wuhan, China). Aβ (DAEFRHDSGYEVHHQKLVF-FAEDVGSNKGAIIGLMVGGVVIA) used in this study were bought from WuHan Dan gang Biological Technology Co., Ltd (Wuhan, China). TNF-α (3707 s), IL-1β (12242 s), GFAP (3670 s), NeuN (94403 s), Iba1 (17198 s), IL-18 (57058 s), PSD95 (2507s), Map2 (4542 s), NF-κB p65 (8242 s), Phospho-NF-κB p65 (3033 s) were purchased from Cell Signaling Technology (Danvers, MA). Phospho-CDK9 (AF4440) was obtained from Affinity (Melbourne, Australia). CDK9 (11,705–1) was obtained from Proteintech (Wuhan, China). HRP-labeled Goat Anti-Mouse IgG (A0216), HRP-labeled Goat Anti-Rabbit IgG (A0208) were purchased from Beyotime (Shanghai, China). Titanium dioxide was purchased from Sigma-Aldrich (13,463–67–7,USA); The information of reagents or resource Table S1. Natural compounds used in this study were showed in Table S2. Anti-inflammatory effects of top 20 natural compounds were showed in Table S3. **S**iCDK9 was synthesized and obtained from Gene Pharma (Suzhou, China).

New object recognition (NOR)

New Object Recognition (NOR) is a widely utilized behavioral test designed to assess memory and cognitive function in rodents. Initially, mice are placed in an empty testing arena to explore freely for 5 mins, allowing them to gain familiarity with the environment. After all the mice have acclimated, two identical rectangular objects (object A) are introduced into the arena. The mice are then allowed to explore these objects for an additional 5 mins to form a memory of them. On the following day, one of the rectangular objects is replaced with a circular object (object B). The mice are reintroduced into the testing arena, and their interactions with each object are recorded, including the time spent exploring each object and the number of contacts made. The cognitive performance of the animals is typically quantified using the Recognition Index (RI), which measures the proportion of time spent on the novel object compared to the familiar one. The RI is calculated using the formula: RI = (Time spent on the novel object) / (Time spent on the novel object + Time spent on the familiar object) × 100 %.

Morris water maze (MWM)

The Morris Water Maze (MWM) is a widely used behavioral experimental technique designed to study spatial learning and memory in rodents. The experimental setup consists of a circular pool with a diameter of 2 m, filled with water made opaque by the addition of a non-toxic substance (Titanium dioxide). The pool is divided into four quadrants. A small, transparent platform is submerged just below the water surface in one of the fixed quadrants and remains in the same position throughout the training period. Prominent visual cues are placed around the room to assist the animals in orienting themselves and navigating to the platform.During the training phase, mice are released from different starting points in the pool and allowed to swim in search of the hidden platform. Each trial continues until the animal locates the platform or until a maximum duration of 60 s elapses. If the mice fails to find the platform within the allotted time, it is gently guided to it. Multiple trials are conducted over several days to facilitate learning. The latency to find the platform, the length of the swim path, and the swim speed are recorded as measures of learning and spatial memory acquisition.Following the training phase, a probe trial is conducted in which the platform is removed from the pool. The mice are then allowed to swim for a fixed duration of 60 s. The primary measure is the amount of time the animals spend in the target quadrant, where the platform was previously located, which reflects their memory of the platform's location.

Immunofluorescent staining (IF)

After fixation in 4 % paraformaldehyde for 24 h, brain tissues were

sequentially incubated in 20 % sucrose solution to replace the paraformaldehyde, followed by sedimentation and replacement with 30 % sucrose solution until tissues settled at the bottom. After removing the sucrose solution, tissues were embedded in OCT compound and frozen using a Leica CM3050 cryostat (Germany) to obtain 15 μm-thick brain sections. Sections were dried for 1 hour, washed three times with 1X PBS, permeabilized with 0.5 % Triton solution for 20 min, and blocked with 10 % BSA for 1 hour. Subsequently, tissues were incubated overnight at 4 °C with appropriate primary antibodies. The following day, tissues were brought to room temperature, incubated with corresponding secondary antibodies for 1 hour, and counterstained with DAPI (Sigma, D6578) for nuclear staining. Imaging was conducted using a Nikon A1 confocal microscope.

Western blot assays

The samples were homogenized and incubated in RIPA lysis and extraction buffer supplemented with a protease and phosphatase inhibitor cocktail (P0013B; Beyotime Biological Technology, Shanghai, China). According to the manufacturer's instructions, protein concentrations were determined using a BCA protein assay kit (A55864, thermofisher,USA). Samples containing equal protein concentrations were loaded onto 12.5 % SDS-PAGE gels and electrophoresed at 300 mA for 1.5 h. The proteins were then transferred onto 0.22 μm PVDF membranes. PVDF membranes with protein bands were blocked with 3 % bovine serum albumin (BSA) at room temperature for 1 hour and subsequently probed with specific primary antibodies (1:1000) overnight at 4 °C. The following day, membranes were washed three times with 1 × TBST (Tris-buffered saline with 0.05 % Tween 20) and incubated with an HRP-conjugated secondary antibody at room temperature for 2 h. Bands were visualized using a chemiluminescence (BCL) assay and band intensities were quantified using Image J software.

Real-time qPCR

Total RNA was isolated from cultured BV2 cells and brain tissues using Trizol reagent (Thermo Fisher, 15,596,026) following standard protocols. RNA concentration was quantified using a spectrophotometer. Subsequently, cDNA synthesis was performed using the PrimeScript RT reagent Kit (Takara, RR037A). The CFX96 Touch Real-time PCR detection system (Bio-Rad) was employed with TB Green Premix Ex Taq II (Takara, RR820A). mRNA expression levels were quantified using the 2ΔΔCt method normalized to GAPDH.

Immunocytochemistry (ICC)

Following drug treatment, BV2 cells were fixed with 4 % paraformaldehyde (PFA) for 20 min. Cells were then incubated with 1X PBS containing 0.1 % Triton X-100 (PBST) for 20 min to enhance cell membrane permeability. Subsequently, cells were blocked with 10 % BSA at room temperature for 1 hour, followed by overnight incubation at 4 °C with primary antibody (1:100). The next day, cells were washed three times with 1X PBS and incubated with fluorescently labeled secondary antibody (1:500) for 2 h. Finally, cells were mounted using an anti-fade fluorescence mounting medium containing DAPI (P0131, Beyotime). Sections were observed and analyzed under a Nikon A1 confocal microscope.

ELISA assay

ELISA (JHN80536, JHN80300, JHN80292, JHN) was performed to assess the release of TNF-α, IL-1β and IL-18 cytokine from BV2 cells treated with Aβ and anti-inflammatory compounds. ELISA was conducted following the manufacturer's instructions. Optical density of each well was measured at 405 nm using an ELISA reader, and cytokine levels were calculated based on the standard curve.

The cellular thermal shift assay (CETSA)

CETSA was utilized to assess the stability of target proteins in cells upon SCL interaction. Cells were harvested and lysed by freeze-thaw cycles using liquid nitrogen. The cell lysates were divided into two fractions and incubated with either DMSO or SCL (100 μM) at 37 °C for 1 hour. Subsequently, the lysates were aliquoted into six PCR tubes and heated at 49 °C, 52 °C, 55 °C, 58 °C, 61 °C, and 64 °C for 3 mins. After cooling at room temperature for 5 mins, the lysates were centrifuged at 20,000 g for 20 mins at 4 °C. The supernatants were collected for protein blot analysis, where equal amounts of protein were loaded.

Drug affinity responsive target stability (DARTS)

DARTS, total protein extraction from cultured cells was performed using protein extraction reagent containing protease and phosphatase inhibitors (NP-40, P0013F, Beyotime) with agitation on ice for 20 min. Subsequently, 10 × TNC buffer (1 M Tris–HCl, 5 ml; 5 M NaCl, 1 ml; 1 M CaCl2, 1 ml; double-distilled H2O, 3 ml; pH 7.4) was added to the cell lysates to achieve a final concentration of 5 μg/μl, followed by gentle mixing. SCL or an equivalent volume of DMSO was added to the cell lysates and incubated at 37 °C for 1 hour. Pronase (dissolved in 1 × TNC buffer; MedChemExpress, HY-114,158) was added at a ratio of 1:1000 to both DMSO and SCL-treated groups and incubated at 37 °C for 15 min. Digestion was stopped by adding 5 × protein loading buffer and boiling the samples for 5 min. Protein analysis was then conducted using Western blotting.

LC-MS/MS

The binding sites of SCL on BV2 cells were detected using LC-MS/MS. Briefly, lysed BV2 cells were incubated with SCL (100 μM) or DMSO for 1 hour at 37 °C. The cell lysates incubated with SCL or DMSO were then separated using SDS-PAGE and stained with Coomassie blue. Peptides were separated on an ultra-high-performance liquid chromatography system (EASY-nLC 1200, Thermo Fisher Scientific, Waltham, Massachusetts, USA) using a linear gradient of solvent A (0.1 % formic acid and 2 % acetonitrile in double-distilled water) and solvent B (0.1 % formic acid and 90 % acetonitrile in double-distilled water). Subsequently, the separated peptides were analyzed using a mass spectrometer (Q Exactive HF, Thermo Scientific, Waltham, Massachusetts, USA) equipped with a nano-electrospray ionization source (2.1 kV). Both precursor and fragment ions were acquired in the Orbitrap at a resolution of 60,000. Protein identification and quantification were performed using Proteome Discoverer 2.4 software for MS data analysis.

Molecular docking

Molecular docking analysis of the selected ligands and targets was performed using the CB-Dock2 platform (https://cadd.labshare.cn/cb-dock2/php/index.php) (Liu et al., 2022). The two-dimensional chemical structure of sclareol was downloaded from the PubChem (https://pubchem.ncbi.nlm.nih.gov/compound/163263) database and then imported into the CB-Dock2 platform to add hydrogen atoms and charges. Simultaneously, the crystal structure of the cyclin-dependent kinase 9 (CDK9) protein (PDB ID: 8K5R) was obtained from the RCSB PDB database and imported into the CB-Dock2 platform to add hydrogen atoms and delete all water molecules. The binding affinity (kcal/mol) was calculated using CB-Dock2, and the optimal docking model with the minimum energy was determined. PyMol 2.5.7 and Discovery Studio 2021 Client software were used to analyze the details of the ligand-receptor interaction and generate 3D and 2D interaction diagrams.

Bio-layer interferometry (BLI)

Label-free kinetic assays were performed using bio-layer interferometry on a BLItz instrument, adhering to the manufacturer's instructions unless otherwise specified. Sensors were soaked and reagents were diluted in kinetics buffer (ForteBio). The assay involved five steps: initial baseline (30 s), loading (180 s), baseline (120 s), association (300 s), and dissociation (300 s). SCL was immobilized onto recombinant human CDK9 (rhCDK9) protein capture biosensors. Sensorgrams were globally fit to a 1:1 binding model using BLItz Pro v1.1.0.28 software. The equilibrium dissociation constant (KD) was determined from at least five different concentrations ranging from 7.8 μM to 125 μM, including a 0 μM control.

Flow cytometry

Apoptosis was measured using the FITC-Annexin V Apoptosis Detection Kit (Beyotime, C1069) according to the manufacturer's protocol. Briefly, cultured cells were harvested, washed with 1xPBS, and resuspended in annexin V-binding buffer. The cells were then gently mixed with FITC-annexin V and propidium iodide (PI) and incubated for 15 min at room temperature in the dark. Following incubation, annexin V^+ and/or PI^+ cells were analyzed by flow cytometry. Data analysis was performed using FlowJo v10.8.1 software.

Statistical analysis

Data analysis was conducted using GraphPad Prism 6.0 software. Data are presented as mean ± SEM. Student's *t*-test was utilized to compare between two groups, while one-way or two-way analysis of variance (ANOVA) with Bonferroni correction was performed for multiple group comparisons. Pearson's correlation coefficient was employed for correlation analysis.

Results

SCL reduced the microglial inflammatory response induced by Aβ

Initially, we conducted a screening of 80 anti-inflammatory compounds to assess their impact on the microglial inflammatory cytokine

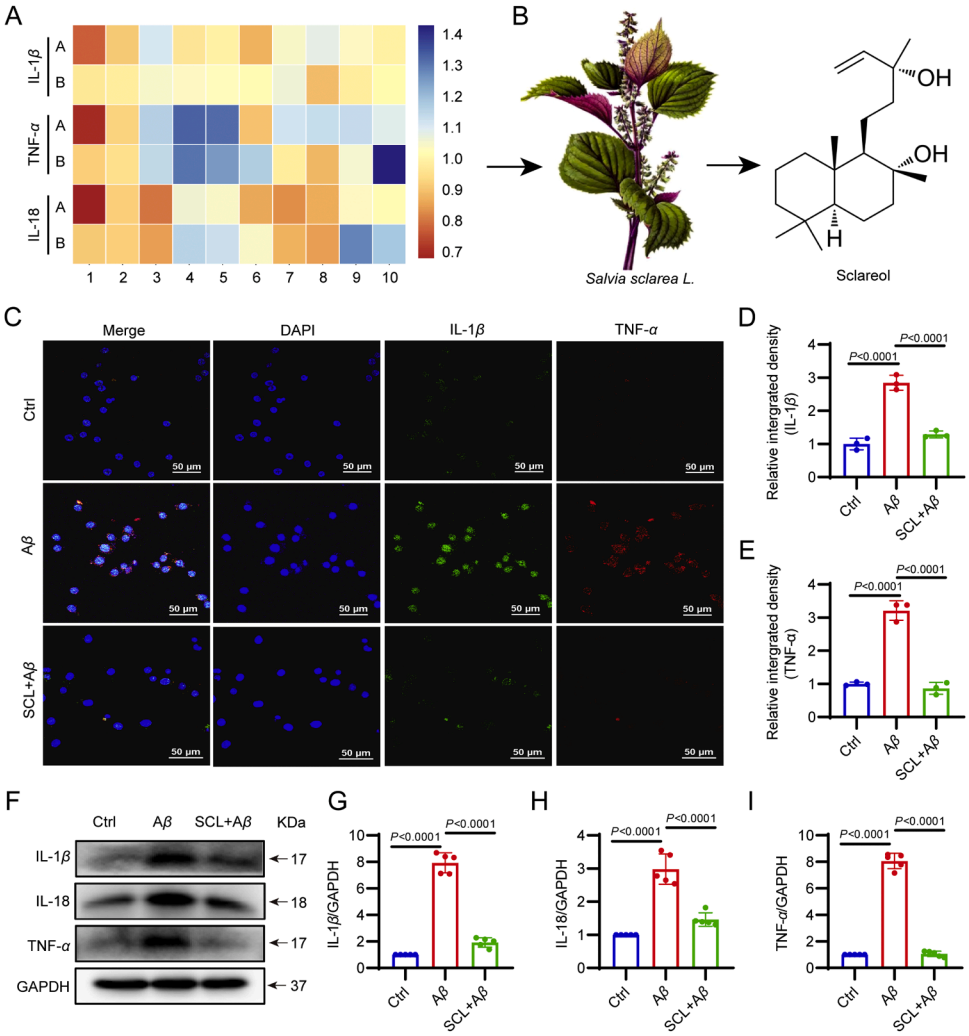

Fig. 1. SCL reduces Aβ-induced microglial inflammation in BV2 cells. (A) SCL effectively alleviates Aβ1–42-triggered inflammation in microglia. BV2 cells were cultured in 96-well plates and pre-treated with 20 natural anti-inflammatory compounds, which are capable of crossing the blood-brain barrier, at specified concentrations. Subsequently, cells were induced with 20 μM Aβ for 24 h. The release of IL-1β, TNF-α and IL-18 were measured using an ELISA assay. (B) The schematic representation and chemical structure of SCL. (C-E) Immunocytochemistry (ICC) staining was performed to detect the inflammatory cytokines TNF-α and IL-1β, with cell nuclei counterstained using DAPI (blue). The scale bar represents 50 μm. (F-I) Western blot analysis was conducted to evaluate the expression levels of IL-1β, IL-18, and TNF-α, in BV2 cells. The band intensities of the corresponding proteins were quantified using Image J software, and the results are presented as mean ± SEM ($n = 5$).

IL-1β, which is induced by Aβ. To do this, BV2 cells were pre-treated with 10 μM of the compound for 2 h and subsequently stimulated with Aβ1–42 (10 μM) for 24 h. The release of IL-1β was measured using an ELISA. Results showed that SCL exhibited better anti-inflammation effect on IL-1β release than other compounds (Fig. S1A). To confirm this result, the top 20 compounds with the most potent anti-inflammatory effects were selected for secondary screening. Release levels of TNF-α and IL-18 were additionally measured by ELISA assays and the results confirmed the significant anti-inflammatory activity of SCL (Fig. 1A). SCL is a diterpene alcohol, rich in glandular trichomes of the calyx, primarily isolated from the inflorescence of *Salvia sclarea l* (Caissard et al., 2012) (Fig. 1B), and has been reported to possess both anti-cancer and anti-inflammatory properties. Subsequently, we used ICC staining (Fig. 1C-E) and western blot analysis (Fig. 1F-I) to further investigate the effects of SCL on Aβ1–42-induced microglial inflammation. Obtained results demonstrated that SCL pretreatment significantly

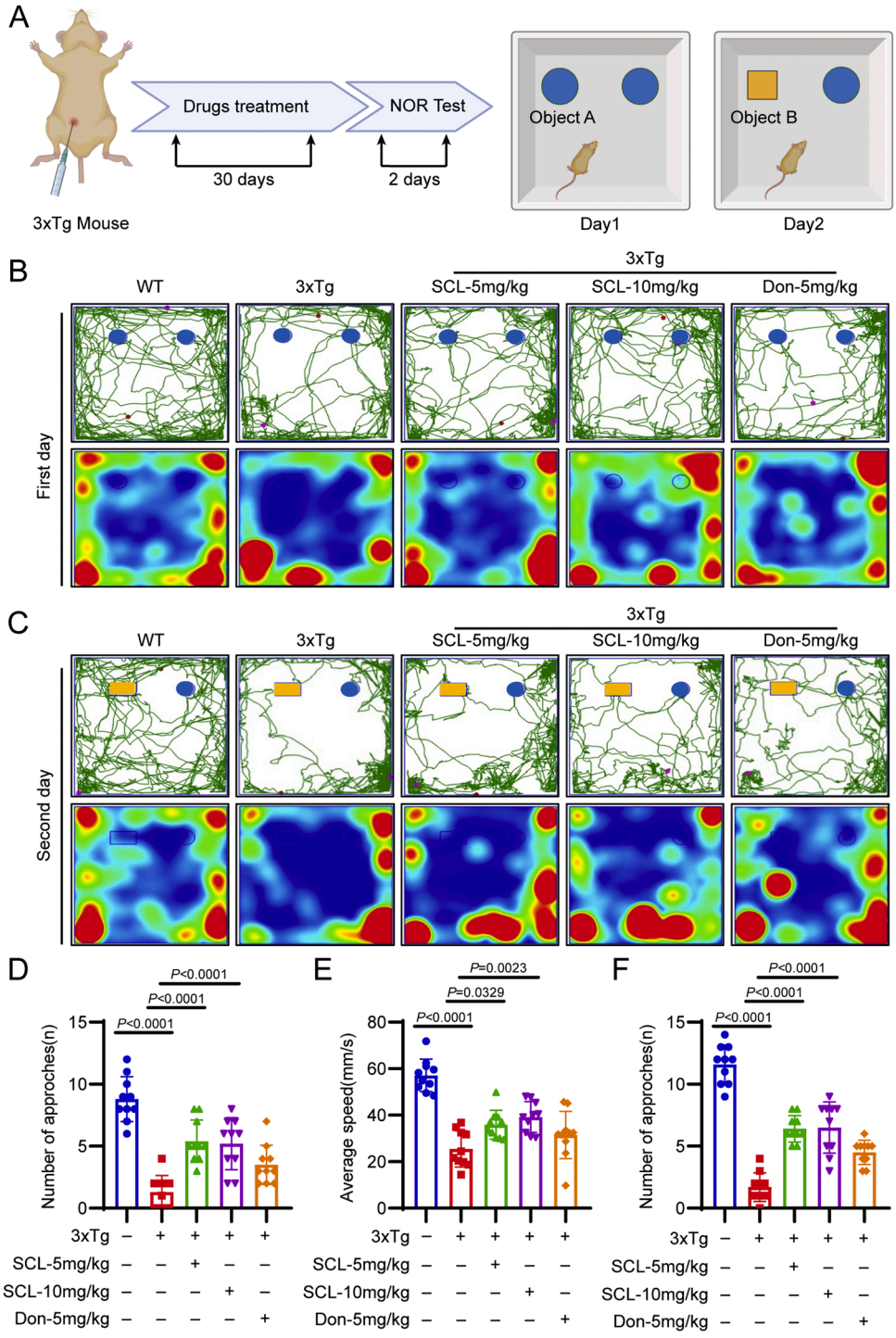

Fig. 2. SCL improves cognitive memory function in 3xTg mice. (A) Eight-month-old 3xTg mice were administered daily intraperitoneal injections of SCL for 30 consecutive days, after which they underwent a two-day novel object recognition (NOR) test. (B-C) Illustrative images from the NOR experiment. (D) Preference for object interaction on the initial day of the novel object recognition test. (E) Average velocity during the initial day of the novel object recognition test. (F) Quantity of interactions with the novel object on the second day of the novel object recognition test. Data are expressed as mean ± SEM for $n = 10$ mice per group.

reduced the release of TNF-α and IL-1β. Furthermore, quantitative PCR (qPCR) results revealed that SCL inhibited the expression of *Tnf-α* and *Il-1β* (Fig. S2A-2B). Noted that SCL possesses the capability to traverse the blood-brain barrier (BBB). To further substantiate the permeability of the BBB, we employed the ADMETlab prediction tool (https://admetmesh.scbdd.com/) and Deep-B3 (https://cbcb.cdutcm.edu.cn/deepb3/), with a predicted probability of 0.784 according to ADMETlab. The result above suggest that SCL may be a good therapeutic agent for targeting microglial inflammation in AD.

SCL improves the cognitive dysfunction in 3 xTg mice

To assess the effects of SCL on learning and memory abilities in 3xTg mice, we conducted a NOR test (Fig. 2A). SCL was administered via intraperitoneal injection (I.P) once daily for 30 consecutive days, with treatments at low (5 mg/kg) and high (10 mg/kg) doses. Donepezil, a clinically approved drug, was administered at a dose of 5 mg/kg and used as a positive control in this experiment. After treatment, we performed NOR test and analyzed the movement trajectories (Fig. 2B-C), number of new object explorations (Fig. 2D), average speed (Fig. 2E), and approach counts (Fig. 2F). The results indicated that exploration of

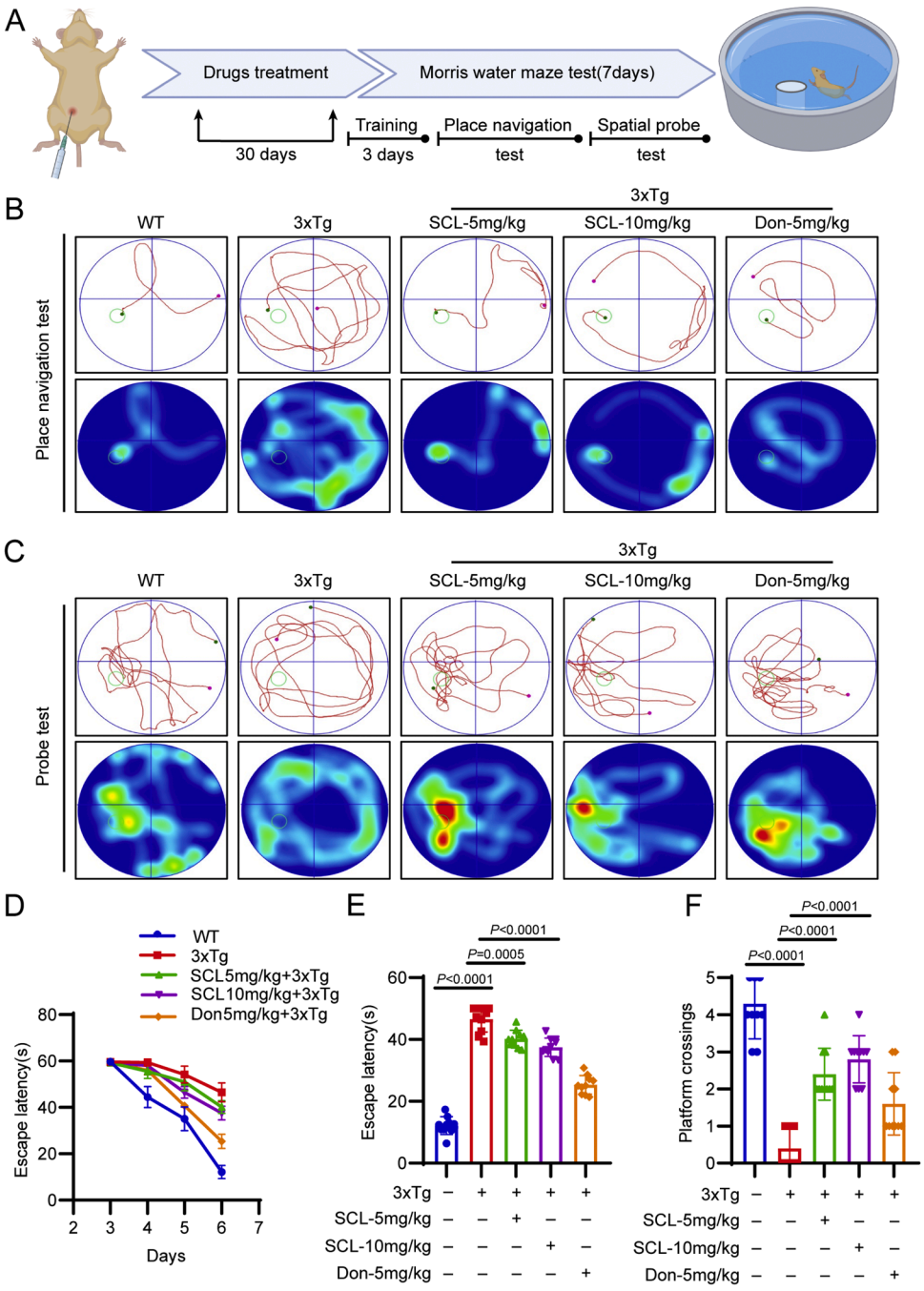

Fig. 3. SCL improves learning and spatial memory deficits in 3xTg mice. (A) Eight-month-old 3xTg mice were administered daily intraperitoneal injections of SCL for 30 consecutive days, followed by a 7-day Morris water maze (MWM) assessment. (B) Representative swim paths from the probe trial on day 6 of the MWM assessment are depicted. (C) Representative swim paths from the probe trial without the hidden platform on day 7 of the Morris water maze assessment. (D) Escape latency outcomes from days 3 to 6 of the Morris water maze assessment. (E) Duration spent in the target quadrant where the platform was situated on day 7. (F) Average number of platform crossings within 60 s for each group of mice on day 7. Data are presented as mean ± SEM of $n = 10$ mice per group.

the novel object was significantly increased in the SCL-treated and donepezil-treated groups compared to the 3xTg group. To further validate our findings, we performed the MWM test (Fig. 3A). The action trajectories of each group of mice were recorded (Fig. 3B-C). Notably, the 3xTg mice exhibited a significant increase in average escape latency, indicating a decline in spatial memory. However, following treatment with SCL or donepezil, the average escape latency was significantly reduced compared to the 3xTg group (Fig. 3D). Furthermore, after the removal of the platform, the SCL-treated and donepezil-treated groups displayed a higher number of platform crossings compared to the 3xTg group (Fig. 3E-F). Interestingly, SCL demonstrated superior efficacy in improving cognitive deficits in 3xTg mice compared to donepezil.

SCL inhibits microglial over-activation and neuronal injury in 3xTg mice

Microglial overactivation-induced neuroinflammation is a hallmark of AD. To investigate the effects of SCL on neuroinflammation and neuronal damage, immunofluorescence (IF) staining was performed to assess the numner of microglial (Iba1), astrocyte(GFAP), and neuron (NeuN) in brain tissues. Notably, administration of SCL or donepezil significantly inhibited the over-activation of both microglia and astrocytes. SCL, at a dose of 10 mg/kg, demonstrated superior efficacy in ameliorating AD pathology compared to the positive control drug, donepezil (Fig. 4A-D). To further confirm the improve effects of SCL on microglial overactivation, western blot (WB) analysis was conducted on tissue homogenates (Fig. 4E-G). The results showed that SCL at a 10 mg/kg dose was more effective than donepezil in suppressing inflammatory cytokines.

SCL directly binds to CDK9

To gain deeper insights into the functional mechanisms of SCL and to precisely identify its direct protein targets, we executed a DARTS experiment aimed at uncovering proteins that SCL potentially modulates within the framework of AD. Mass spectrometry analysis has identified 931 prospective SCL-interacting proteins (Fig. 5A). Subsequently, we performed cluster analysis using the STRING database on proteins that were not expressed in the DMSO group but were highly expressed in the SCL-treated group. Scoring of the core cluster proteins identified CDK9 as the top candidate (Fig. 5B). CDK9, a serine/threonine kinase, plays a crucial role in the regulation of inflammation. CDK9 modulates the activity of Nuclear Factor κB (NF-κB) (Liu et al., 2017), a key transcription factor responsible for the expression of numerous pro-inflammatory genes. Through the activation of the NF-κB signaling pathway, CDK9 contributes to the synthesis of various inflammatory cytokines, including tumor necrosis factor-α (TNF-α), interleukin-1β (IL-1β), and interleukin-6 (IL-6). This regulatory function highlights CDK9 as an important mediator in inflammatory responses.

To validate the binding of SCL to CDK9, we conducted biolayer interferometry (BLI) assays. The results confirmed the interaction between SCL and CDK9, with a dissociation constant (Kd) of 8.80×10^{-4} M, indicating a strong binding affinity of SCL for CDK9 (Fig. 5C). To strengthen the evidence for our findings, we integrated both DARTS and immunoblotting methods in our analysis. Results demonstrated that SCL specifically inhibited CDK9 degradation by pronase (Fig. 5D-E). Furthermore, we performed cellular thermal shift assays (CETSA) to assess the stability of CDK9 in the presence of SCL. The findings indicated that CDK9 in the DMSO group underwent denaturation at 64 °C, whereas its stability was marginally preserved in the presence of SCL at the same temperature.(Fig. 5F-G). Finally, molecular docking analysis indicated potential binding sites at GLN-27 and ILE-25, providing insights into the interaction between SCL and CDK9 (Fig. 5H).

SCL targets CDK9 to regulate the downstream NF-κB signaling pathway

To further explore whether SCL suppresses Aβ-induced CDK9 phosphorylation and mitigates neuroinflammation by targeting CDK9. Upon conducting a western blot analysis on tissue homogenates, it was revealed that administering SCL at a dosage of 10 mg/kg demonstrated superior efficacy in suppressing the phosphorylation of CDK 9 and its subsequent target, P-NF-κB65 (P65), when compared to the positive control drug, donepezil (Fig. 6A-C). Similarly, pretreatment with SCL thwarted the Aβ-induced phosphorylation of CDK9 and P65 in BV2 cells, effectively preventing the associated cellular changes (Fig. 6D-F). Considering that nuclear translocation of the P65 protein is a pivotal event in the activation of the NF-κB pathway, we also quantified the levels of P65 within the nuclear and cytosolic compartments. Our results demonstrated that SCL reduces Aβ-induced P65 nuclear translocation, thereby modulating the NF-κB inflammatory pathway (Fig. 6G). In summary, these results suggest that SCL modulates the NF-κB pathway through direct interaction with CDK9, suppressing its phosphorylation activity, and thus impedes neuroinflammation triggered by Aβ.

SCL modulates neuroinflammation and neuronal injury via CDK9-NFκB axis

To validate the pivotal role of CDK9 in the modulation of neuroinflammation by SCL, we transfected BV2 cells with CDK9-targeting siRNA (si-CDK9) and confirmed the efficiency of CDK9 silencing (Fig. 7A-B). Western blot analysis was subsequently performed to evaluate the phosphorylation of the downstream target P65 and the release of inflammatory cytokines. The results revealed that silencing CDK9 in conjunction with SCL pretreatment inhibited Aβ-induced phosphorylation of P65 and the release of TNF-α and IL-1β to a similar extent as SCL pretreatment alone, with no observed additive effect (Fig. 7C-F).

Microglial activation and inflammation-mediated neurotoxicity are recognized as key factors in the pathogenesis of AD. To assess the impact of microglia-derived inflammatory factors on neuronal cells, we prepared conditioned media from BV2 cells. BV2 cells were exposed to Aβ for 6 h, washed with 1x PBS, and then incubated in 10 % DMEM for 24 h to collect the conditioned media. HT22 cells were then treated with this microglia-conditioned media for 24 h to evaluate the inflammatory environment's effect on neuronal cells (Fig. 7G). The results demonstrated that conditioned media from Aβ-exposed microglia increased apoptosis and intracellular ROS production in HT22 cells (Fig. 7H-I). In contrast, conditioned medium from microglia with CDK9 silencing did not cause damage to HT22 cells, and there was no significant difference in ROS release and cell apoptosis compared to the SCL pretreatment group. In summary, these results suggest that SCL exerts control over neuroinflammation and neuronal damage through its direct interaction with CDK9, which in turn suppresses the CDK9-NFκB signaling pathway.

Discussion

In this study, we demonstrated that SCL significantly inhibited the release of inflammatory factors, improved neuronal damage, and ultimately alleviated cognitive dysfunction and pathology in AD model mice. Mechanistically, SCL exerted its protective effects by binding to CDK9, which results in the inhibition of the downstream NF-κB signaling pathway. This action improves the imbalance of the inflammatory environment in the brain and mitigating AD pathology.

Neuroinflammation has emerged as a pivotal contributor to the underlying mechanisms of AD (Althafar, 2022; Zhang et al., 2020). Microglia, as the resident immune cells of the brain, occupy a crucial position in maintaining brain homeostasis. This includes preserving the structural integrity of the central nervous system, defending it against harmful pathogens, and continuously scrutinizing the brain parenchyma. However, in AD, microglia lose their homeostatic function (Althafar, 2022). As a consequence of this impairment, microglia display aberrant activation patterns, initiating a cascade of inflammatory responses and neuronal damage, which significantly contribute to the progression of neurodegeneration observed in AD (Schroder and

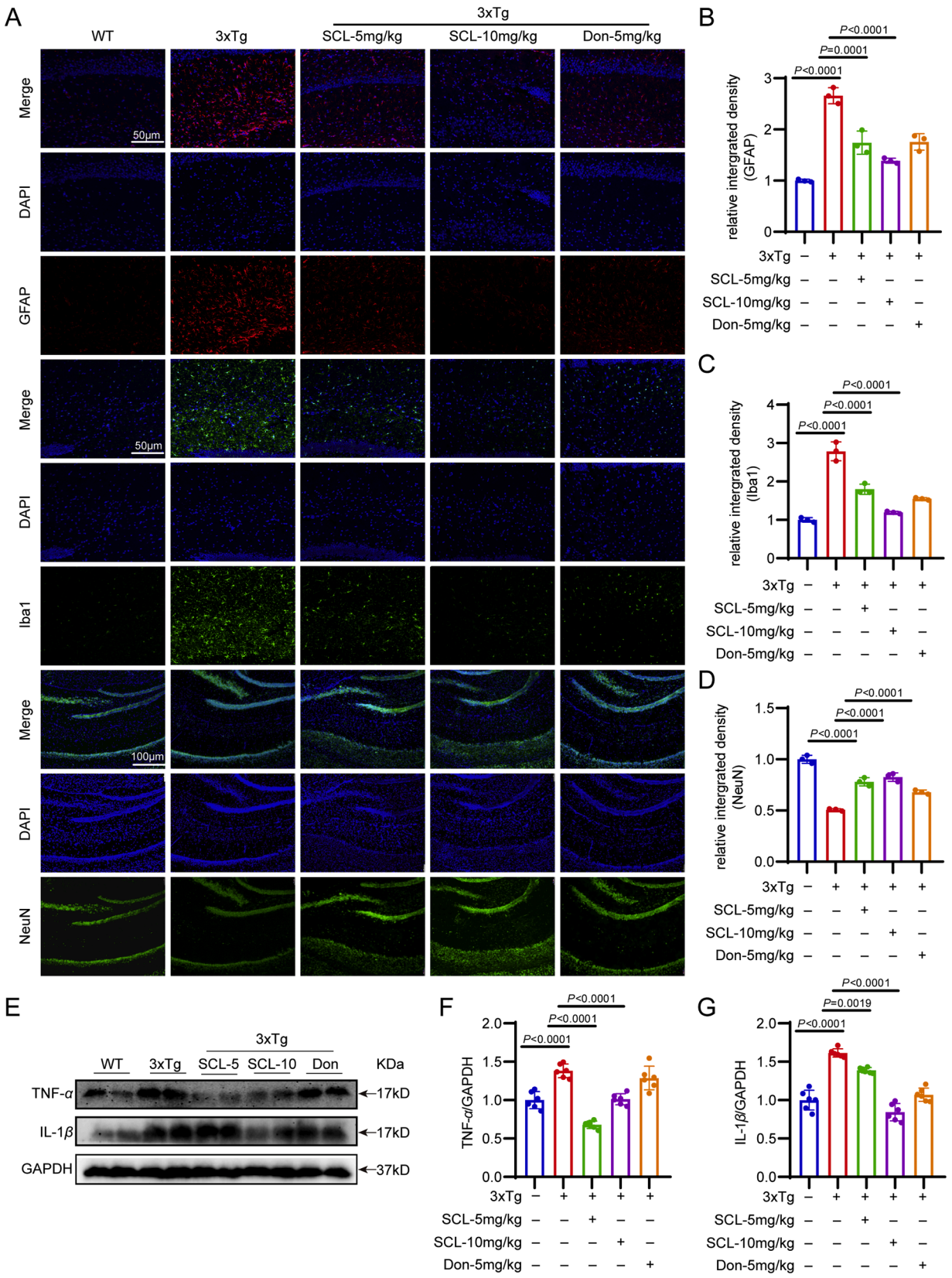

Fig. 4. The SCL treatment diminished the activation of glial cells and the loss of neurons in 3xTg mice. (A) Displayed are representative images of GFAP, Iba1, and NeuN staining within the hippocampal region, accompanied by a scale bar measuring 100 μm. (B-D) The average fluorescence intensity was measured using Image J, and the outcomes are depicted as mean ± SEM ($n = 3$). (E) Also shown is a representative Western blot analysis of TNF-α and IL-1β in the hippocampus, with GAPDH serving as a loading control. (F-G) The quantification of band intensities for the respective proteins was carried out using Image J, and the results are presented as mean ± SEM ($n = 6$).

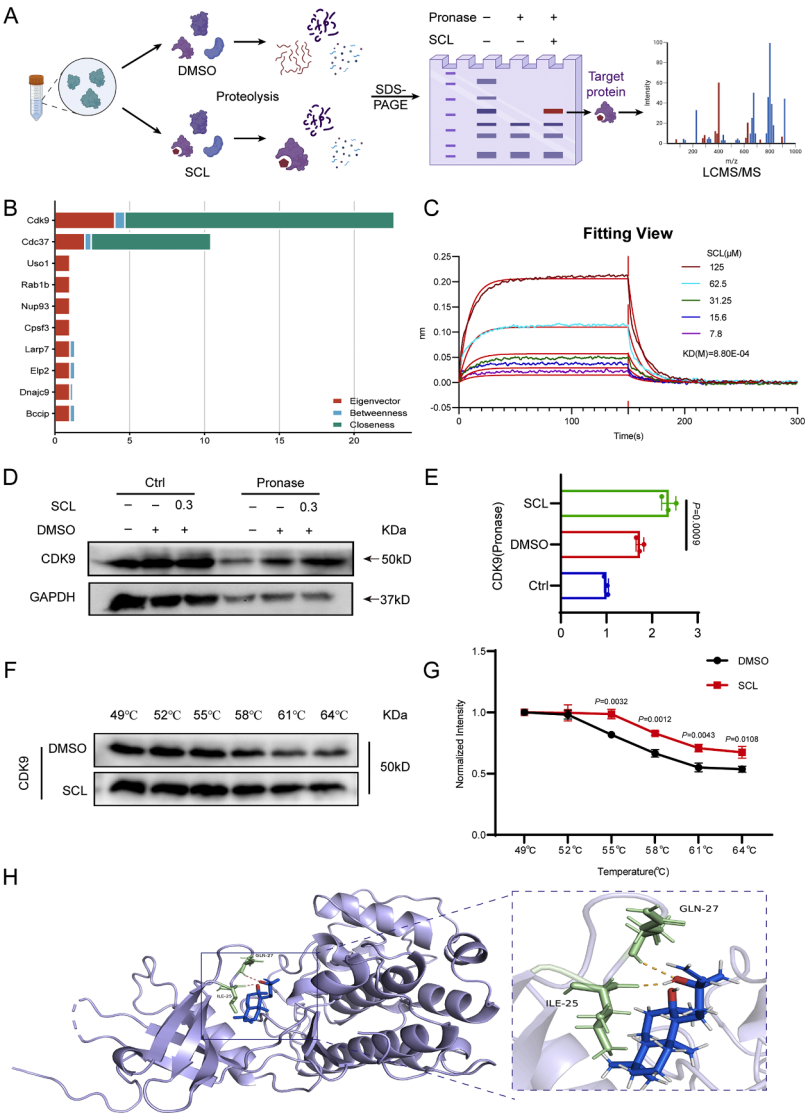

Fig. 5. SCL directly binds to CDK9. (A) A schematic illustration of the combined DARTS (Drug Affinity Responsive Target Stability) and LC-MS/MS approach. (B) Mass spectrometry analysis indicated that CDK9 displayed the most robust interaction with SCL. (C) Bio-layer interferometry (BLI) analysis confirmed a direct binding between SCL and CDK9, with the average KD constant calculated from five separate experiments. (D) BV2 cells were lysed and subjected to incubation with SCL overnight at 4 °C. DARTS analysis was conducted using pronase (20 ng/μg protein), succeeded by immunoblotting of the lysates. (E) Band intensity quantification for the corresponding proteins was executed using ImageJ, with outcomes presented as mean ± SEM ($n = 3$). (F-G) CETSA was utilized to evaluate the impact of SCL (1000 nmol/l) on the thermal stability of CDK9 within BV2 cell lysates ($n = 3$). The statistical outcomes, with DMSO serving as the control, are depicted and presented as mean ± SEM. (H) The three-dimensional binding model of CDK9 with SCL. The backbone of CDK9 and the structure of SCL are illustrated. Residues in CDK9 are depicted as cyan sticks, while residues in SCL are shown as red sticks. Hydrogen bonds are denoted by yellow dashed lines.

Tschopp, 2010). Moreover, the dysregulated microglia also fail to efficiently clear away damaged neurons and debris, leading to the accumulation of harmful proteins and other cellular remnants. This build-up creates a toxic environment that perpetuates the cycle of neurodegeneration and exacerbates cognitive decline (Selkoe, 2002; von Bernhardi et al., 2015). Thus, the overactivtion of microglia represents a crucial step in the pathogenesis of AD (Dimas et al., 1999). It underscores the need for therapeutic strategies aimed at restoring microglial overactivation and mitigating their detrimental effects on neuronal health. By targeting microglia-mediated inflammation and clearance mechanisms, we may be able to slow down the progression of AD and improve the quality of life for those affected by this disease.

Natural products are the main source of modern innovative drugs (Atanasov et al., 2021), with numerous compounds demonstrating therapeutic effects across a wide range of inflammatory diseases, including rheumatoid arthritis (Gandhi et al., 2021), atopic dermatitis (Wang et al., 2024), inflammatory bowel disease (Meng et al., 2024), ulcerative colitis (Ruan et al., 2024) and neurodegenerative disease (Li et al., 2024), etc. Among the promising compounds identified luteolin (He et al., 2023), urolithin a (Hou et al., 2024), and artemisinin b (Qiang et al., 2018) have exhibited potential, primarily in neuroprotection and addressing mitochondrial dysfunction. However, their effects on microglia, the brain's resident immune cells, have been less explored. SCL, a naturally occurring compound derived from *Salvia sclarea*, emerged from our screening as a potent anti-inflammatory agent with the ability to modulate microglial activation. What distinguishes SCL from other candidates is its reported ability to cross the BBB following oral administration (Dimas et al., 1999), making it particularly promising for CNS disorders like AD, where drug delivery is often a critical challenge. In the study, SCL not only inhibited the release of pro-inflammatory factors from microglia but also ameliorated neuronal damage, resulting in improved cognitive function and a reduction in

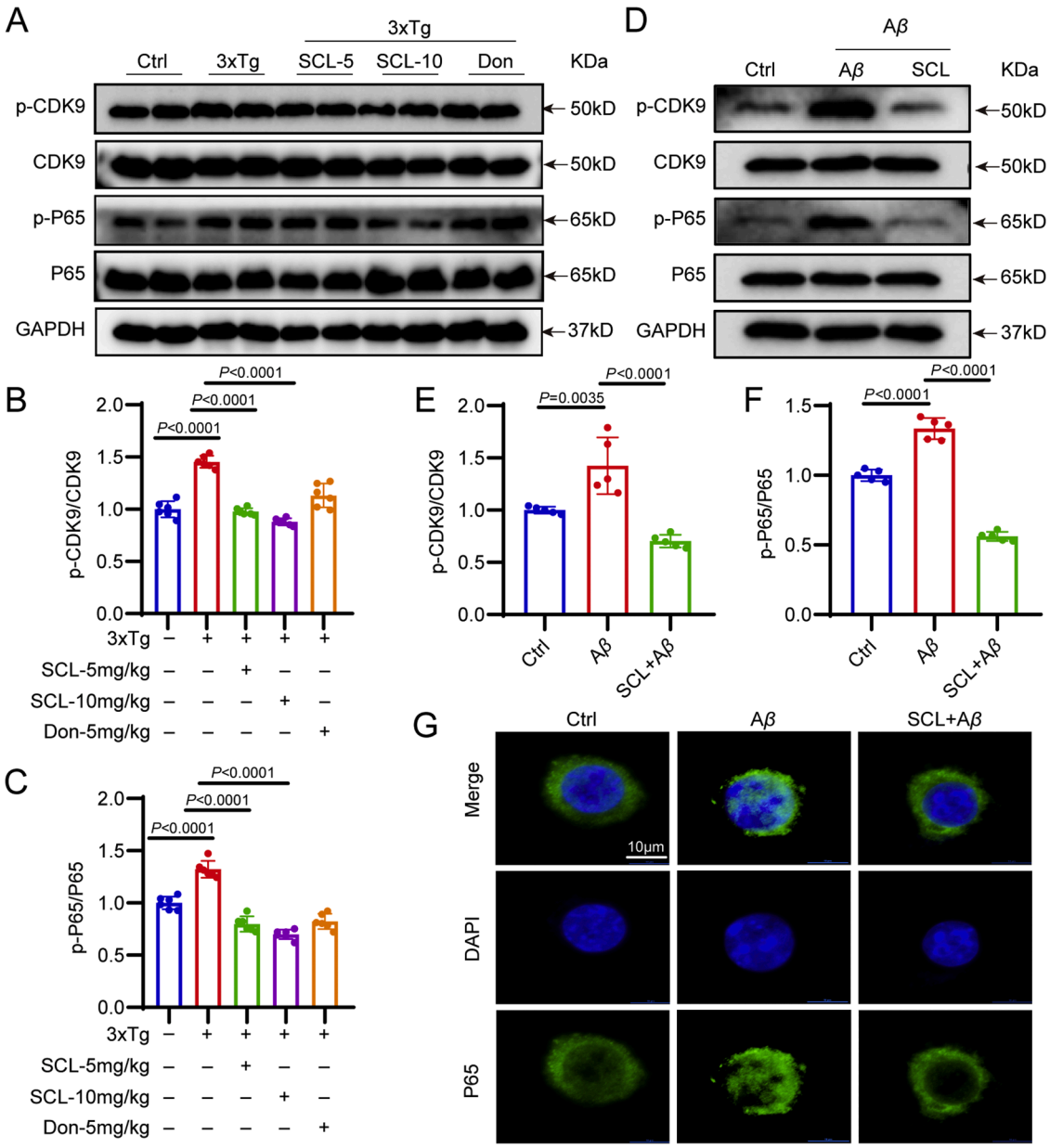

Fig. 6. SCL modulates the phosphorylation of CDK9 and its downstream NFκB pathways. (A-C) Representative Western blot analysis of p-CDK9, CDK9, p-NFκB p65, and NFκB p65 in mouse brain tissue lysates. (D-F) Representative Western blot analysis of p-CDK9, CDK9, p-NFκB p65, and NFκB p65 in BV2 cells pretreated with SCL and subsequently exposed to 20 μM Aβ for 24 h. (G) Representative immunofluorescence staining of NFκB p65 (green) in BV2 cells, with or without SCL pretreatment, following exposure to 20 μM Aβ for 24 h [scale bar = 10 μm].

pathological features in AD model mice. These findings highlight SCL's therapeutic potential, particularly in targeting microglia-mediated inflammation, a central process in the progression of AD.

Through a comparative analysis of MCODE scores for the top ten proteins identified via LC-MS/MS, we identified CDK9 and cell division cycle 37 homolog (CDC37) as the two substrates with the highest binding potential to SCL. CDC37 is a known regulator of the cell cycle, primarily involved in maintaining the stability and activity of various protein kinases (Gray et al., 2007). However, its specific role in mediating anti-inflammatory effects remains largely unexplored. In contrast, CDK9, a kinase regulated by cell cycle-dependent mechanisms, has been extensively implicated in inflammation and its downstream signaling cascades (Hellvard et al., 2016; Sangsuwan et al., 2022), as well as in the pathogenesis of AD (Yin et al., 2023). The phosphorylation and dephosphorylation of CDK9 at key sites throughout the transcription process require tight regulation (Nekhai et al., 2014). Furthermore, CDK9 plays a pivotal role in modulating NF-κB, a transcription factor celebrated for its central role in inflammatory responses (Schmerwitz et al., 2011), regulates the expression of a vast array of genes involved in immune and inflammatory responses. Its activation is tightly controlled and can be triggered by various stimuli, such as pathogens, cytokines, and stress signals. Upon activation, NF-κB translocates to the nucleus, where it binds to specific DNA sequences and initiates the transcription of target genes. CDK9 facilitates the transcription of NF-κB-dependent genes by enhancing the elongation phase of transcription. This results in the increased expression of cytokines, chemokines, and other mediators of inflammation, contributing to the amplification and perpetuation of the inflammatory response. Our findings revealed that SCL binds directly to CDK9, inhibiting its phosphorylation, which in turn modulates the pro-inflammatory activity of NF-κB. This mechanism contributes to the reduction of neuroinflammation and alleviates AD-related pathology.

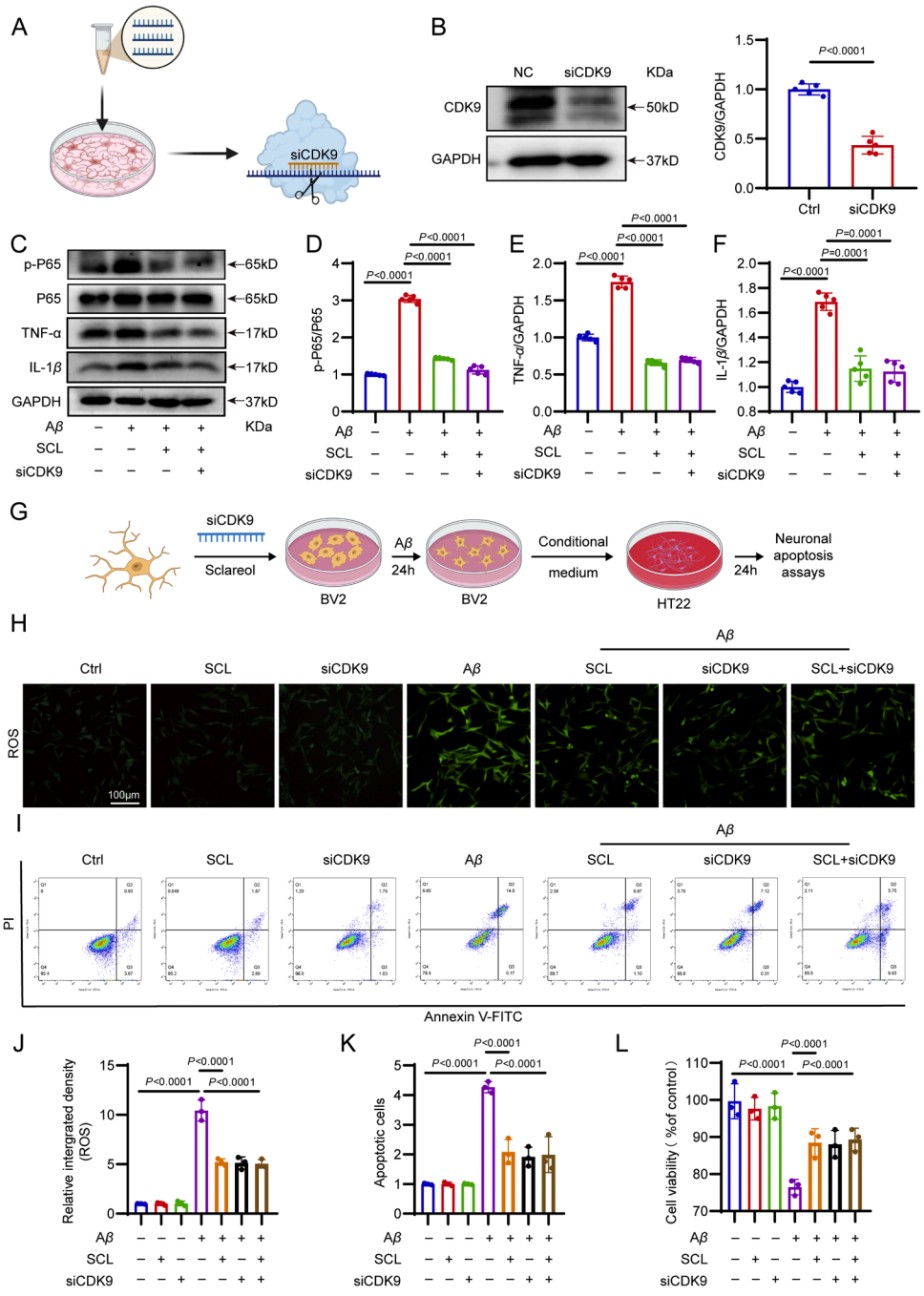

Fig. 7. Inhibiting CDK9 activity suppresses neuroinflammation and neuronal cell death. (A) Diagram illustrating the siRNA transfection process. (B) Western blot analysis demonstrating the knockdown of CDK9 in BV2 cells. Cells were subjected to transfection with either negative control siRNA (NC) or CDK9-targeting siRNA (siCDK9), using GAPDH as a loading control (data are expressed as mean ± SEM; $n = 3$). (C-F) Western blot analysis of phosphorylated NFκB p65, total NFκB p65, TNF-α, and IL-1β levels in BV2 cells after CDK9 siRNA transfection. Post-transfection, cells were exposed to 5 μM SCL for 2 h, followed by 20 μM Aβ for 24 h. Data are presented as mean ± SEM ($n = 3$). (G) Diagram depicting the preparation of conditioned media. (H) Representative images of ROS staining to assess intracellular ROS levels, with a scale bar of 100 μm. (I) Flow cytometry images showing apoptotic cells. (J) The average fluorescence intensity was measured using Image J, and the outcomes are depicted as mean ± SEM ($n = 3$). (K) Quantitative analysis of (I). (L) MTT assay results to evaluate cell viability.

Conclusion

In conclusion, our research emphasizes that SCL serves as a powerful inhibitor of microglia-induced neuroinflammation, offering substantial neuroprotective benefits in AD models. By directly binding to CDK9 and inhibiting its phosphorylation, SCL targets the NF-κB signaling pathway, effectively diminishing the secretion of pro-inflammatory cytokines. These findings emphasize SCL as a potential candidate for the treatment of AD.

CRediT authorship contribution statement

Hao Tang: Writing – original draft, Formal analysis, Data curation. **Luyao Li:** Methodology, Data curation. **Qin Yu:** Data curation. **Linjie Chen:** Data curation. **Xiaoxia Xu:** Data curation. **Ziyao Meng:** Data curation. **Yuqing Zeng:** Investigation. **Fan Chen:** Data curation. **Hammad Muzaffar:** Data curation. **Wei Wang:** Methodology. **Xia Zhao:** Writing – review & editing, Funding acquisition, Conceptualization. **Guang Liang:** Writing – review & editing, Supervision, Funding

acquisition.

Declaration of competing interest

The authors declare that they have no known competing financial interests or personal relationships that could have appeared to influence the work reported in this paper.

Acknowledgments

The study was supported by a grant from the Zhejiang Provincial Key Scientific Project (2021C03041 to G.L.), and Medical and health Science and Technology Project of Zhejiang Province (2025KY1032 to X.Z.). Basic Scientific Research Funds of Department of Education of Zhejiang Province (KYYB202010 to F.C.).

Supplementary materials

Supplementary material associated with this article can be found, in the online version, at doi:10.1016/j.phymed.2025.156504.

References

Akiyama, H., Barger, S., Barnum, S., Bradt, B., Bauer, J., Cole, G.M., Cooper, N.R., Eikelenboom, P., Emmerling, M., Fiebich, B.L., Finch, C.E., Frautschy, S., Griffin, W. S., Hampel, H., Hull, M., Landreth, G., Lue, L., Mrak, R., Mackenzie, I.R., McGeer, P. L., O'Banion, M.K., Pachter, J., Pasinetti, G., Plata-Salaman, C., Rogers, J., Rydel, R., Shen, Y., Streit, W., Strohmeyer, R., Tooyoma, I., Van Muiswinkel, F.L., Veerhuis, R., Walker, D., Webster, S., Wegrzyniak, B., Wenk, G., Wyss-Coray, T., 2000. Inflammation and Alzheimer's disease. Neurobiol. Aging 21, 383–421.

Althafar, Z.M., 2022. targeting microglia in Alzheimer's disease: from molecular mechanisms to potential therapeutic targets for small molecules. Molecules. 27.

Atanasov, A.G., Zotchev, S.B., Dirsch, V.M., , International Natural Product Sciences, T., Supuran, C.T., 2021. Natural products in drug discovery: advances and opportunities. Nat. Rev. Drug Discov. 20, 200–216.

Bappi, M.H., Mia, M.N., Ansari, S.A., Ansari, I.A., Prottay, A.A.S., Akbor, M.S., El-Nashar, H.A.S., El-Shazly, M., Mubarak, M.S., Torequl Islam, M., 2024. Quercetin increases the antidepressant-like effects of sclareol and antagonizes diazepam in thiopental sodium-induced sleeping mice: a possible GABAergic transmission intervention. PhytOther Res. 38, 2198–2214.

Caissard, J.C., Olivier, T., Delbecque, C., Palle, S., Garry, P.P., Audran, A., Valot, N., Moja, S., Nicole, F., Magnard, J.L., Legrand, S., Baudino, S., Jullien, F., 2012. Extracellular localization of the diterpene sclareol in clary sage (Salvia sclarea L., Lamiaceae). PLoS. One 7, e48253.

Casey, D.A., Antimisiaris, D., O'Brien, J., 2010. Drugs for Alzheimer's disease: are they effective? P. T. 35, 208–211.

Colonna, M., Butovsky, O., 2017. Microglia function in the central nervous system during health and neurodegeneration. Annu. Rev. Immunol. 35, 441–468.

DeTure, M.A., Dickson, D.W., 2019. The neuropathological diagnosis of Alzheimer's disease. Mol. Neurodegener. 14, 32.

Dimas, K., Kokkinopoulos, D., Demetzos, C., Vaos, B., Marselos, M., Malamas, M., Tzavaras, T., 1999. The effect of sclareol on growth and cell cycle progression of human leukemic cell lines. Leuk. Res. 23, 217–234.

Gandhi, G.R., Jothi, G., Mohana, T., Vasconcelos, A.B.S., Montalvao, M.M., Hariharan, G., Sridharan, G., Kumar, P.M., Gurgel, R.Q., Li, H.B., Zhang, J., Gan, R. Y., 2021. Anti-inflammatory natural products as potential therapeutic agents of rheumatoid arthritis: a systematic review. Phytomedicine 93, 153766.

Glass, C.K., Saijo, K., Winner, B., Marchetto, M.C., Gage, F.H., 2010. Mechanisms underlying inflammation in neurodegeneration. Cell 140, 918–934.

Gray Jr., P.J., Stevenson, M.A., Calderwood, S.K., 2007. Targeting Cdc37 inhibits multiple signaling pathways and induces growth arrest in prostate cancer cells. Cancer Res. 67, 11942–11950.

He, Z., Li, X., Wang, Z., Cao, Y., Han, S., Li, N., Cai, J., Cheng, S., Liu, Q., 2023. Protective effects of luteolin against amyloid beta-induced oxidative stress and mitochondrial impairments through peroxisome proliferator-activated receptor gamma-dependent mechanism in Alzheimer's disease. Redox. Biol. 66, 102848.

Hellvard, A., Zeitlmann, L., Heiser, U., Kehlen, A., Niestroj, A., Demuth, H.U., Koziel, J., Delaleu, N., Jan, P., Mydel, P., 2016. Inhibition of CDK9 as a therapeutic strategy for inflammatory arthritis. Sci. Rep. 6, 31441.

Hou, Y., Chu, X., Park, J.H., Zhu, Q., Hussain, M., Li, Z., Madsen, H.B., Yang, B., Wei, Y., Wang, Y., Fang, E.F., Croteau, D.L., Bohr, V.A., 2024. Urolithin A improves Alzheimer's disease cognition and restores mitophagy and lysosomal functions. Alzheimers. Dement. 20, 4212–4233.

Knopman, D.S., Amieva, H., Petersen, R.C., Chetelat, G., Holtzman, D.M., Hyman, B.T., Nixon, R.A., Jones, D.T., 2021. Alzheimer disease. Nat. Rev. Dis. Primers. 7, 33.

Li, T., Li, Y., Chen, J., Nan, M., Zhou, X., Yang, L., Xu, W., Zhang, C., Kong, L., 2024. Hyperibone J exerts antidepressant effects by targeting ADK to inhibit microglial P2X7R/TLR4-mediated neuroinflammation. J. Adv. Res.

Liu, T., Zhang, L., Joo, D., Sun, S.C., 2017. NF-kappaB signaling in inflammation. Signal. Transduct. Target. Ther. 2, 17023. -.

Liu, Y., Yang, X., Gan, J., Chen, S., Xiao, Z.X., Cao, Y., 2022. CB-Dock2: improved protein-ligand blind docking by integrating cavity detection, docking and homologous template fitting. Nucleic. Acids. Res. 50, W159–W164.

Lopez-Rodriguez, A.B., Hennessy, E., Murray, C.L., Nazmi, A., Delaney, H.J., Healy, D., Fagan, S.G., Rooney, M., Stewart, E., Lewis, A., de Barra, N., Scarry, P., Riggs-Miller, L., Boche, D., Cunningham, M.O., Cunningham, C., 2021. Acute systemic inflammation exacerbates neuroinflammation in Alzheimer's disease: iL-1beta drives amplified responses in primed astrocytes and neuronal network dysfunction. Alzheimers. Dement. 17, 1735–1755.

McKhann, G.M., Knopman, D.S., Chertkow, H., Hyman, B.T., Jack Jr., C.R., Kawas, C.H., Klunk, W.E., Koroshetz, W.J., Manly, J.J., Mayeux, R., Mohs, R.C., Morris, J.C., Rossor, M.N., Scheltens, P., Carrillo, M.C., Thies, B., Weintraub, S., Phelps, C.H., 2011. The diagnosis of dementia due to Alzheimer's disease: recommendations from the National Institute on Aging-Alzheimer's Association workgroups on diagnostic guidelines for Alzheimer's disease. Alzheimers. Dement. 7, 263–269.

Meng, Q., Guo, J., Lv, K., Liu, Y., Zhang, J., Li, M., Cheng, X., Chen, S., Huo, X., Zhang, Q., Chen, Y., Li, J., 2024. 5S-Heudelotinone alleviates experimental colitis by shaping the immune system and enhancing the intestinal barrier in a gut microbiota-dependent manner. Acta Pharm. Sin. B 14, 2153–2176.

Nekhai, S., Petukhov, M., Breuer, D., 2014. Regulation of CDK9 activity by phosphorylation and dephosphorylation. Biomed. Res. Int. 2014, 964964.

Qiang, W., Cai, W., Yang, Q., Yang, L., Dai, Y., Zhao, Z., Yin, J., Li, Y., Li, Q., Wang, Y., Weng, X., Zhang, D., Chen, Y., Zhu, X., 2018. Artemisinin B improves learning and memory impairment in AD dementia mice by suppressing neuroinflammation. Neuroscience 395, 1–12.

Ransohoff, R.M., Perry, V.H., 2009. Microglial physiology: unique stimuli, specialized responses. Annu. Rev. Immunol. 27, 119–145.

Ruan, Y., Zhu, X., Shen, J., Chen, H., Zhou, G., 2024. Mechanism of Nicotiflorin in San-Ye-Qing rhizome for anti-inflammatory effect in ulcerative colitis. Phytomedicine 129, 155564.

Sangsuwan, R., Yik, J.H.N., Owen, M., Liu, G.Y., Haudenschild, D.R., Lewis, J.S., 2022. Intra-articular injection of flavopiridol-loaded microparticles for treatment of post-traumatic osteoarthritis. Acta Biomater. 149, 347–358.

Scheltens, P., De Strooper, B., Kivipelto, M., Holstege, H., Chetelat, G., Teunissen, C.E., Cummings, J., van der Flier, W.M., 2021. Alzheimer's disease. Lancet 397, 1577–1590.

Schmerwitz, U.K., Sass, G., Khandoga, A.G., Joore, J., Mayer, B.A., Berberich, N., Totzke, F., Krombach, F., Tiegs, G., Zahler, S., Vollmar, A.M., Furst, R., 2011. Flavopiridol protects against inflammation by attenuating leukocyte-endothelial interaction via inhibition of cyclin-dependent kinase 9. Arterioscler. Thromb. Vasc. Biol. 31, 280–288.

Schroder, K., Tschopp, J., 2010. The inflammasomes. Cell 140, 821–832.

Schwartzentruber, J., Cooper, S., Liu, J.Z., Barrio-Hernandez, I., Bello, E., Kumasaka, N., Young, A.M.H., Franklin, R.J.M., Johnson, T., Estrada, K., Gaffney, D.J., Beltrao, P., Bassett, A., 2021. Genome-wide meta-analysis, fine-mapping and integrative prioritization implicate new Alzheimer's disease risk genes. Nat. Genet. 53, 392–402.

Selkoe, D.J., 2002. Alzheimer's disease is a synaptic failure. Science (1979) 298, 789–791.

Tarkowski, E., Andreasen, N., Tarkowski, A., Blennow, K., 2003. Intrathecal inflammation precedes development of Alzheimer's disease. J. Neurol. Neurosurg. Psychiatry 74, 1200–1205.

von Bernhardi, R., Eugenin-von Bernhardi, L., Eugenin, J., 2015. Microglial cell dysregulation in brain aging and neurodegeneration. Front. Aging Neurosci. 7, 124.

Wang, C., Chen, S., Guo, H., Jiang, H., Liu, H., Fu, H., Wang, D., 2022a. Forsythoside A mitigates Alzheimer's-like pathology by inhibiting ferroptosis-mediated neuroinflammation via Nrf2/GPX4 axis activation. Int. J. Biol. Sci. 18, 2075–2090.

Wang, H., Xie, M., Rizzi, G., Li, X., Tan, K., Fussenegger, M., 2022b. Identification of sclareol as a natural neuroprotective Ca(v) 1.3-antagonist using synthetic parkinson-mimetic gene circuits and computer-aided drug discovery. Adv. Sci. (Weinh) 9, e2102855.

Wang, R.X., Zhou, M., Ma, H.L., Qiao, Y.B., Li, Q.S., 2021. The role of chronic inflammation in various diseases and anti-inflammatory therapies containing natural products. ChemMedChem. 16, 1576–1592.

Wang, Y., Lu, H., Cheng, L., Guo, W., Hu, Y., Du, X., Liu, X., Xu, M., Liu, Y., Zhang, Y., Xi, R., Wang, P., Liu, X., Duan, Y., Zhu, J., Li, F., 2024. Targeting mitochondrial dysfunction in atopic dermatitis with trilinolein: a triacylglycerol from the medicinal plant Cannabis fructus. Phytomedicine 132, 155856.

Wright, A.L., Zinn, R., Hohensinn, B., Konen, L.M., Beynon, S.B., Tan, R.P., Clark, I.A., Abdipranoto, A., Vissel, B., 2013. Neuroinflammation and neuronal loss precede Abeta plaque deposition in the hAPP-J20 mouse model of Alzheimer's disease. PLoS. One 8, e59586.

Yang, Z., Zhou, D.D., Huang, S.Y., Fang, A.P., Li, H.B., Zhu, H.L., 2023. Effects and mechanisms of natural products on Alzheimer's disease. Crit. Rev. Food Sci. Nutr. 63, 3168–3188.

Yin, L., Zhou, J., Li, T., Wang, X., Xue, W., Zhang, J., Lin, L., Wang, N., Kang, X., Zhou, Y., Liu, H., Li, Y., 2023. Inhibition of the dopamine transporter promotes lysosome biogenesis and ameliorates Alzheimer's disease-like symptoms in mice. Alzheimers. Dement. 19, 1343–1357.

Zhang, Y., Zhao, Y., Zhang, J., Yang, G., 2020. Mechanisms of NLRP3 inflammasome activation: its role in the treatment of Alzheimer's disease. Neurochem. Res. 45, 2560–2572.